HHS Public Access

Author manuscript

NMR Biomed. Author manuscript; available in PMC 2017 December 01.

Published in final edited form as:

NMR Biomed. 2016 December ; 29(12): 1670–1677. doi:10.1002/nbm.3617.

Fast diffusion kurtosis imaging (DKI) with Inherent COrrelation-based Normalization (ICON) enhances automatic segmentation of heterogeneous diffusion MRI lesion in acute stroke

Iris Yuwen Zhou[1,‡], **Yingkun Guo**[1,2,‡], **Takahiro Igarashi**[1], **Yu Wang**[1,3], **Emiri Mandeville**[4], **Suk-Tak Chan**[1], **Lingyi Wen**[1,2], **Mark Vangel**[1], **Eng H Lo**[4], **Xunming Ji**[3], and **Phillip Zhe Sun**[1,2,3,4,*]

[1]Athinoula A. Martinos Center for Biomedical Imaging, Department of Radiology, Massachusetts General Hospital and Harvard Medical School, Charlestown, MA, USA

[2]Department of Radiology, West China Second University Hospital, Sichuan University, Chengdu, Sichuan, China

[3]China-America joint neuroscience institute, Xuanwu Hospital, Capital Medical University, Beijing

[4]Neuroprotection Research Laboratory, Department of Radiology and Neurology, Massachusetts General Hospital and Harvard Medical School, Charlestown, MA, USA

Abstract

Diffusion kurtosis imaging (DKI) has been shown to augment DWI for defining irreversible ischemic injury. However, the complexity of cerebral structure/composition makes kurtosis map heterogeneous, limiting the specificity of kurtosis hyperintensity to acute ischemia. We proposed an Inherent COrrelation-based Normalization (ICON) analysis to suppress the intrinsic kurtosis heterogeneity for improved characterization of heterogeneous ischemic tissue injury. Fast DKI and relaxation measurements were performed on normal (N=10) and stroke rats following MCAO (N=20). We evaluated the correlations between mean kurtosis (MK), mean diffusivity (MD), fractional anisotropy (FA) derived from fast DKI sequence and relaxation rates of R_1 and R_2, and found highly significant correlation between MK and R_1 ($P<0.001$). We showed that ICON analysis suppressed the intrinsic kurtosis heterogeneity in the normal cerebral tissue, enabling automated tissue segmentation in an animal stroke model. We found significantly different kurtosis and diffusivity lesion volumes, being 147±59 and 180±66 mm^3, respectively ($P=0.003$, Paired-t test). The ratio of kurtosis to diffusivity lesion volume was 84±19% ($P<0.001$, One-sample t-test). We found relaxation normalized MK (RNMK) but not MD values significantly different between kurtosis and diffusivity lesions ($P<0.001$, ANOVA). Our study showed that fast DKI with ICON analysis provides a promising means for demarcating heterogeneous DWI stroke lesion.

Graphical Abstract

*Corresponding author: Phillip Zhe Sun, Ph.D. (pzhesun@mgh.harvard.edu), 149 13th Street, Rm 2301, Charlestown, MA 02129, United States, Athinoula A. Martinos Center for Biomedical Imaging, Department of Radiology, MGH and Harvard Medical School, Phone: 617-726-4060, Fax: 617-726-7422.

‡These authors contributed equally.

Kurtosis augments DWI for defining irreversible ischemic injury. However, the complexity of cerebral structure/composition makes kurtosis map heterogeneous, limiting the specificity of kurtosis hyperintensity to acute ischemia. With strong correlation found between mean kurtosis and R_1, we proposed an Inherent COrrelation-based Normalization (ICON) approach to mitigate the kurtosis heterogeneity in normal brain with substantially reduced scan time. We further demonstrated that this approach enabled automatic lesion segmentation and enhanced stratification of heterogeneous DWI lesion, aiding the translation of fast DKI to the acute stroke setting.

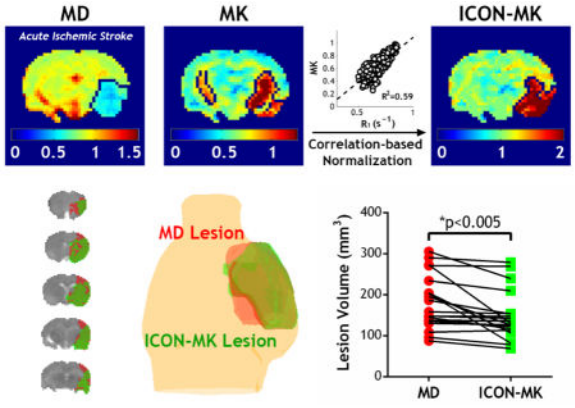

Keywords

Acute Stroke; Diffusion kurtosis imaging (DKI); Mean diffusivity (MD); Inherent COrrelation-based Normalization (ICON); Relaxation normalized mean kurtosis (RNMK); K-means Clustering

1. INTRODUCTION

Diffusion-weighted imaging (DWI) is sensitive to early ischemic tissue injury, and can detect ischemic lesion within minutes of the ischemic insult. Given its advantage in early detection of acute stroke, DWI has become one of the most widely used MRI techniques for stroke imaging (1–4). Various mismatch paradigms, including perfusion/diffusion, angiogram/diffusion and clinical/diffusion where the NIH Stroke Scale (NIHSS) used as a clinical indicator of infarction volume, have been proposed to guide stroke treatment beyond the standard therapeutic window (5–8). However, it has been recognized that ischemic tissue damage within the DWI lesion is heterogeneous (9–15). A portion of the DWI lesion represents injury that is reversible when reperfusion is prompt and effective, and the extent of DWI lesion reversibility is independently associated with improved outcome (16–19). As such, the underlying assumption that the DWI lesion identifies the irreversibly injured ischemic core is oversimplified, and advanced imaging techniques are urgently needed to refine diffusion stroke MRI (20).

Diffusion kurtosis imaging (DKI) has been introduced as a method to quantify non-Gaussian diffusion and has been applied to a number of neurological disorders including Parkinson’s disease, Huntington’s disease, traumatic brain injury and stroke (21–31). It has been shown that there is significant mismatch between mean diffusivity (MD) and mean kurtosis (MK) lesions in an animal model of acute stroke (32). In addition, diffusivity lesion without

kurtosis abnormality responds favorably to early reperfusion, where little change is found in the kurtosis lesion, suggesting that the kurtosis abnormality captures the more severely damaged ischemic core and hence, stratifies the conventional DWI lesion. However, unlike the relatively homogeneous trace diffusion image, the complexity of cerebral structure and composition leads to a heterogeneous kurtosis map, in which the specificity of kurtosis abnormality to ischemia is compromised, making automatic lesion segmentation somewhat difficult. A means to minimize the intrinsic cerebral tissue kurtosis variation would thus enhance the conspicuity of the ischemic kurtosis lesion.

The conventional DKI protocol requires collecting DWI images with multiple b-values along at least fifteen directions, resulting in relatively long acquisition time (21). Recently, a fast DKI protocol has been introduced by Hansen et al. for the rapid mapping of MD and MK (33,34). The diffusivity and kurtosis maps obtained with the fast DKI agreed well with those estimated from conventional DKI using the diffusion tensor model (MD_{tensor} and MK_{tensor}) in normal brain (33), in glioma (35) and importantly in acute stroke brain (33,34,36). We have further shown that kurtosis is one of the most sensitive indices in capturing acute ischemic lesion (37). Herein we developed a relaxation-normalized fast DKI approach to refine acute ischemic lesion stratification. Briefly, we evaluated the correlation between cerebral MK and multiple MRI indices including MD, fractional anisotropy (FA), and relaxation (R_1, R_2). There were significant correlation between MK and R_1, MK and R_2, and MK and FA, with R_1 showing the highest correlation coefficient. Because MD and FA may alter substantially during acute stroke while the change in relaxation rate is relatively small, we proposed an Inherent COrrelation-based Normalization (ICON) analysis and validated it in suppressing the intrinsic kurtosis heterogeneity. We demonstrated that the ICON approach enabled automatic ischemic lesion segmentation during acute ischemic stroke, superior to the MK-based lesion analysis. In summary, our study developed relaxation-normalized fast kurtosis imaging for characterizing heterogeneous ischemic tissue injury, aiding the translation of fast diffusion kurtosis imaging to the acute stroke setting.

2. MATERIALS AND METHODS

Animals

All experiments have been approved by the Institutional Animal Care and Use Committee. Adult male Wistar rats (Charles River Laboratory, Wilmington, MA) were anesthetized throughout the surgery and the MRI experiments with 1.5–2.0% isoflurane/air mixture. Animal body temperature was maintained by a circulating warm water jacket positioned around the torso. We imaged ten normal rats (N=10) and twenty three stroke rats following the standard permanent middle cerebral artery occlusion (MCAO, N=23). Briefly, MCAO was induced by inserting a 4–0 silicon-coated nylon suture (Doccol Corp, Sharon, MA) into the lumen of the right internal carotid artery, and then advancing it to block the origin of the middle cerebral artery. Stroke rats were then transferred to the MRI scanner after the surgery and imaged 1.5 to 2 hours after the onset of occlusion. Peripheral oxygen saturation (SpO2) and heart rate were continuously monitored (Nonin Pulse Oximeter 8600, Plymouth, MN). The SpO2 was not significantly different between the two groups, being 95 ± 4 % (normal)

vs. 92 ± 3 % (MCAO). Three animals were excluded from analysis due to failed MCAO surgery.

MRI

MRI data were acquired using a 4.7 Tesla small-bore MRI scanner (Bruker Biospec, Billerica, MA). We used a dual RF coil setup, including a 70 mm volume transmitter coil and an actively-decoupled 20 mm surface receiver coil. During MRI, the animals were placed on a plastic cradle with the head fixed with a tooth bar and ear bars to minimize motion. Multi-slice MRI (5 slices, slice thickness/gap = 1.8/0.2 mm, field of view = 20×20 mm^2, acquisition matrix = 48×48) was acquired with single-shot echo-planar imaging (EPI) (receiver bandwidth = 225 kHz), with the central slice positioned at 2 mm posterior to bregma. Fast DKI was acquired using three b-values: one b = 0 s/mm^2 image, nine b = 1000 s/mm^2 and nine b = 2500 s/mm^2 images along directions of $\hat{n}^{(i)}$, $\hat{n}^{(i+)}$, $\hat{n}^{(i)}$ (i.e. $\hat{n}^{(i)} = (0,1,1)^T$, $\hat{n}^{(1+)} = (0,1,1)^T$, and $\hat{n}^{(1-)} = (0,1,-1)^T$, and similarly for i =2 and 3) (38). Note that the superscript i in $\hat{n}^{(i)}$ labels the position of the "1" while in $\hat{n}^{(i+)}$ and $\hat{n}^{(i-)}$ it labels the position of the "0" (33,34). The other parameters of the fast DKI approach were gradient pulse duration/diffusion time (δ/Δ) = 6/20 ms, repetition time (TR)/echo time (TE) = 2500/36.6 ms, 4 averages, scan time = 3 min 10 s. In addition, T_1-weighted images were acquired using an inversion recovery sequence, with seven inversion delays ranging from 250 to 3000 ms (TR/TE = 6500/14.8 ms, 4 averages, scan time = 3 min 38 s); T_2-weigthed SE images were obtained with two TEs of 30 and 100 ms (TR = 3250 ms, 4 averages, scan time = 26 s). Perfusion imaging was acquired with amplitude modulated arterial spin labeling MRI (TR/TS/TE = 6500/3250/14.8 ms, 32 averages, scan time = 7 min).

Image and Data Analysis

Images were analyzed in MATLAB (MathWorks, Natick, MA). MD and MK maps were obtained by linear combination of log diffusion signals, as described previously (33,34,36,37,39). FA was estimated based on standard diffusion tensor model. In addition, parametric T_1 map was derived using least-squares fitting of the signal as functions of inversion time ($I = I_0 \lfloor 1 - (1-\eta)e^{-TI/T_1} \rfloor$), where η is the inversion efficiency, TI is the inversion time, and I_0 is equilibrium signal. T_2 map was calculated as $T_2 = \frac{TE_2 - TE_1}{\ln(I(TE_1)/I(TE_2))}$, where $I(TE_{1,2})$ are T_2-weighted signals obtained at different echo times (TE= 30 and 100 ms). The relationship between MK and other MRI indices (T_1, T_2, MD and FA) was evaluated using Pearson's correlation, excluding ventricular area with MD value above 1 $\mu m^2/ms$. An estimated MK map (MK_{est}) was calculated using the regression coefficients determined from the univariate linear regression analysis between R_1 and MK per pixel (i.e. $MK_{est} = C_0 + C_1 * R_1$, where C_0 and C_1 are regression coefficients) and then the relaxation-normalized MK (RNMK) map was calculated as $RNMK = MK/MK_{est}$. Cerebral blood flow (CBF) map was obtained from amplitude modulated arterial spin labeling MRI (40) and derived as $CBF = \frac{\lambda (I_{ref} - I_{tag})}{2\alpha \cdot I_{ref}} \cdot \frac{e^{w/T_{1a}}}{T_{1w}}$, where I_{tag} is the label image, I_{ref} is the reference image, λ is the brain-blood partition coefficient for water, α is the degree of inversion with transient time correction, w is the post-labeling delay, and T_{1a} is the arterial blood longitudinal relaxation time (41).

Results were expressed as mean ± standard deviation (S.D.). We evaluated the association between MK and relaxation, MD and FA with univariate and multiple linear regressions, and *P*-values of less than 0.05 were considered statistically significant. The size of ischemic lesions in MD, MK or RNMK maps were automatically defined using a K-means clustering-based algorithm (42). Briefly, a 1D vector of all the pixels within the brain was formed and clustering algorithm used an iterative refinement technique to partition the data points in the vector into two clusters (lesion vs. normal tissue) based on their intensities.

3. RESULTS

Fig. 1 shows parametric brain T_1, T_2, MD, FA, and MK maps from a representative normal Wistar rat. Because cerebral spinal fluid (CSF) has significantly higher water content, the ventricle region appears hyperintense in T_1, T_2 and MD images. In addition, CSF displays hypointensity in FA and MK maps due to little anisotropic/restricted diffusion. Whereas the contrast between striatum or corpus callosum regions and cortical region was relatively small in T_2 and MD maps, it was distinct in T_1, FA and MK maps. This suggests that kurtosis, a measure of non-Gaussian diffusion, is partially associated with diffusion fractional anisotropy, a widely-used measure of gross white matter microstructure (43–45) along with longitudinal relaxation rate, which has been shown to be associated with semisolid macromolecules and water content (46,47).

We evaluated the relationship between MK and other MRI indices using Pearson's correlation with a Student's t-distribution, excluding ventricular regions using an MD threshold of 1 $\mu m^2/ms$ (Fig. 2a). There was a weak correlation between MK and MD (R^2=0.11, P<0.001), consistent with previous report suggesting that diffusivity and kurtosis are two distinct diffusion-based indices for characterizing tissue microstructure (48). The pixel-wise analysis also showed a weak correlation between MK and FA (R^2=0.17, P<0.001), moderate correlation between MK and R_2 (=1/T_2, R^2=0.37, P<0.001) and strong correlation between MK and R_1 (=1/T_1, R^2=0.70, P<0.001). The correlation between MK and R_1 was significantly higher than that between MK and MD, FA or R_2 in normal animals (N=10, ANOVA with multiple comparison test, P<0.001). Because MD and FA may change substantially during acute stroke, we compared the univariate linear regression of MK and R_1 versus multiple linear regression of MK with R_1 and R_2 in all the normal animals (Fig. 2b). We found that the coefficient of determination (i.e., R^2) was 0.62 ± 0.08 (MK and R_1, P<0.001) and 0.62 ± 0.08 (MK, R_1 and R_2, P<0.001), showing little difference (Two-sample t-test, P=0.92). Hence, we chose the univariate linear regression of MK and R_1 to correct for intrinsic kurtosis heterogeneity in intact cerebral tissue.

Fig. 3 compares the routine MK and relaxation-normalized MK maps in a normal Wistar rat. Both the relaxation R_1 (i.e., 1/T_1) map (Fig. 3a) and the MK map (Fig. 3b) show hyperintensity in striatum and corpus callosum. Fig. 3c shows the estimated MK map (MK_{est}) using the regression coefficients determined from univariate linear regression analysis between R_1 (Fig. 3a) and MK (Fig. 3b) per pixel (MK_{est}= 1.42*R_1-0.26). Fig. 3d shows the proposed relaxation-normalized MK map (i.e. RNMK=MK/MK_{est}), which was substantially more homogeneous than the MK map without relaxation normalization (Fig. 3a). For all the normal animals studied, the coefficient of variation (COV, i.e., S.D./mean)

was 23.6 ± 2.3% and 12.1 ± 2.8% for MK and RNMK maps, respectively. This represents 48.6 ± 10.2% decrease in COV, showing that the ICON analysis removes a substantial portion of kurtosis heterogeneity which is intrinsic to normal cerebral tissue.

We further evaluated the ICON analysis in a representative acute stroke animal within 2 hrs after ischemia. R_1 (Fig. 4a) and R_2 (Fig. 4b) maps show relatively small change during acute ischemic stroke, with a reduction of 1.8 % in R_1 and 0.1% in R_2 in the ischemic lesion. In comparison, substantial reduction in MD map was observed in the ischemic lesion (Fig. 4c). The diffusivity lesion was 42.7 mm^3 for the slice. The MK map is heterogeneous, particularly in the internal capsule and striatum, which leads to overestimated kurtosis lesion (Fig. 4d). While the ipsilateral cortex shows relatively increased kurtosis from that of the contralateral cortex, the K-means clustering algorithm missed part of the cortex lesion but incorrectly included the contralateral internal capsule and ipsilateral striatum to the kurtosis lesion (Fig. 4d, arrows), resulting in kurtosis lesion substantially larger than the diffusivity lesion (54.2 vs. 42.7mm^3). Fig. 4e demonstrates significant correlation between R_1 and MK indices from the contralateral normal brain (R^2=0.59, P<0.001). For the contralateral brain, MK and RNMK values were found to be 0.67 ± 0.13 and 1.00 ± 0.12, respectively. This represents a relative COV decrease of 42%, similar to that found in intact brains. The kurtosis lesion was segmented from RNMK map, using the K-means clustering algorithm (Fig. 4f). Compared to the lesion segmented in Fig. 4d which inaccurately includes part of the contralateral normal tissue, the ICON analysis corrected for such error and resulted in a kurtosis lesion size of 41 mm^3, which is close to but slightly smaller than the MD lesion (as seen in Fig. 4c and 4f).

We further tested relaxation-normalized kurtosis analysis for multi-slice segmentation in acute stroke rats. Fig. 5a shows the outlined diffusivity and kurtosis lesions superimposed on a scout scan, in which diffusivity and kurtosis lesions appear in red and green, respectively. Fig. 5b shows substantial kurtosis/diffusivity mismatch. Fig. 5c compares diffusivity and kurtosis lesion volumes in all stroke animals. Specifically, we found kurtosis lesion significantly smaller than that of diffusivity lesion (147±59 vs. 180±66 mm^3, P=0.003, Paired-t test). The ratio of kurtosis to diffusivity lesion volumes was 84±19% (P<0.001, One-sample t-test). Moreover, we compared the CBF, MD, RNMK values in different brain regions including contralateral normal, diffusivity lesion, kurtosis lesion and their mismatch (Table 1). MD was 0.63±0.06 and 0.65±0.06 μm^2/ms in diffusivity and kurtosis lesions (n.s., ANOVA) while their RNMK values were significantly different (1.60±0.27 vs. 1.77±0.21, P<0.05, ANOVA). The kurtosis/diffusivity lesion mismatch had a relatively higher MD value (p<0.05, ANOVA) while its RNMK value was significantly lower than that of diffusivity lesion (p<0.001, ANOVA) and kurtosis lesion (p<0.001, ANOVA). Our results demonstrated that relaxation-normalized kurtosis imaging effectively reduced the intrinsic kurtosis heterogeneity, enabling automatic tissue segmentation of acute stroke DKI.

4. DISCUSSION

Our results demonstrated significant correlation between mean kurtosis and longitudinal relaxation, and that relaxation-normalized fast DKI reduces the intrinsic kurtosis heterogeneity, facilitating automatic segmentation of heterogeneous ischemic tissue. In

addition, we showed that there was no statistically significant difference in mean diffusivity between diffusivity and kurtosis lesions, consistent with prior studies that showed the DWI lesion cannot be reliably characterized based solely on the severity of diffusion coefficient deficit (16). Our prior work showed that in an animal model of acute stroke, diffusivity and kurtosis lesion mismatch responds favorably to early reperfusion with little change in the kurtosis lesion, demonstrating that kurtosis index may resolve heterogeneous DWI lesion (32). However, because of the intrinsic heterogeneity between structures in the MK map, lesions were manually outlined. Our study here developed a relaxation-normalized MK analysis for automatic lesion segmentation, and confirmed significant acute stroke diffusivity and kurtosis lesion mismatch. It is important to note that kurtosis change is sensitive to complex origins including multi-compartment diffusion, restricted diffusion and tortuosity, etc. It is likely that the diffusivity/kurtosis lesion mismatch is subject to intracellular/extracellular net water shift following trans-membrane ion channel dysfunction while kurtosis lesion undergoes pronounced intracellular tortuosity and viscosity elevation, precursors of the irreversible cell damage (49–51).

The proposed ICON analysis utilized the strong correlation between MK and R_1 to suppress the intrinsic kurtosis heterogeneity. We evaluated the R_1 and R_2 rates of all the stroke animals and found that ischemic lesion as defined by MD deficit showed relatively small R_1 decrease compared to that of the normal side, being only 3.6 ± 2.2 % ($P<0.01$), and no detectable changes in R_2 ($P=0.74$), consistent with prior studies (52,53). Meanwhile, ICON analysis shows a substantial increase in the lesion with an average change of around 17% in the kurtosis/diffusivity mismatch area and it goes to as high as 77% in the kurtosis lesion and 60% in the diffusivity lesion. As such, the ICON approach performs well for acute stroke imaging.

We used a fast DKI protocol to minimize the acute stroke scan time (33,34). Our previous work has demonstrated significant correlation of kurtosis measured by the routine DKI protocol and the fast DKI method in an animal model of acute stroke (36). Recently we also showed that MK is one of the most sensitive parameters in revealing acute ischemic injury when compared to radial and axial kurtosis, MD and FA (37). Although our study acquired additional six images at b=1000 s/mm^2 for fractional anisotropy calculation, these additional images can be omitted in the future due to the weak correlation between MK and FA.

Our study demonstrated significant yet relatively weak correlations between kurtosis, FA and transverse relaxation rate. More importantly, we showed that longitudinal relaxation alone accounts for approximately 49% of kurtosis heterogeneity in normal brain. Kurtosis measures non-Gaussian diffusion behavior, which is strongly related to tissue microstructure (e.g., macromolecules, membranes and fibers) that creates diffusion barriers and compartments (25,39). A large diffusional kurtosis suggests a high degree of diffusional heterogeneity and/or microstructural complexity. This is particularly evident in brain, where water diffusion is strongly restricted by myelinated axons. On the other hand, longitudinal relaxation time T_1 highly correlates with magnetization transfer ratio (MTR), an index sensitive to macromolecules (47). T_1 is also closely related to tissue myelination (54,55) and in particular, the cholesterol that is bound to myelin (56). In addition, T_1 was found to be associated with tissue water content (46,57). It is likely that macromolecules, myelin and/or

water content may affect multiple MRI indices of healthy brain, which may partially explain the correlation among the measurements. Additional MRI indices such as magnetization transfer (MT) and amide proton transfer MRI which contain information about the chemical and physical environments of macromolecular protons in tissue may further enhance the correlation (58–60) and hence improve suppression of intrinsic heterogeneity in kurtosis map and specificity of MK changes to ischemic tissue injury. It is necessary to point out that multi-parametric MRI acquisition beyond the highly correlated T_1 and kurtosis MRI will prolong the scan time, limiting its use during acute stroke imaging. Techniques such as fingerprinting MRI may make the proposed approach more applicable in the emergency settings (61).

Accurate identification of the salvageable ischemic tissue is crucial in the clinical settings, particularly with the recent advancement in embolectomy. In this work, we studied acute ischemic tissue injury within 2 hours from occlusion using a well-established filament MCAO model. This time window is similar to the hyperacute phase of stroke patients, which is the most critical period for effective treatment. Although reasonably reproducible, the filament model induces severe hypoperfusion and, arguably, significantly reduces the salvageable tissue and shortens the treatment window. This limitation may be reasonably addressed by using an embolic stroke model, albeit its moderately higher variability (62). Another advantage of using the embolic model is that it enables evaluation of thrombolytic therapy that mimics recanalization in stroke patients. More importantly, our method can be used to study the irreversible and reversible ischemic lesion in the embolic model with thrombolytic treatment, especially beyond the hyperacute window before significant T_1 change occurs, potentially extending the treatment window. On the other hand, there may be substantial relaxation changes in the ischemic lesion at extended stroke onset time, which can be largely attributable to edema formation. The performance of ICON approach in subacute stroke imaging needs to be investigated in the future. In the current study, no histology was obtained because commonly used Hematoxylin and eosin (H&E) and TTC staining techniques cannot reliably identify acute ischemic tissue injury. Notably, before we can investigate histological changes, we need to develop a reliable lesion segmentation approach to guide histology, which is the goal of our current study. It would be interesting to confirm the tissue classification and reversibility of ischemic brain using more sensitive immunohistological techniques in the future.

In this study, we chose a relatively short diffusion time, which is desirable given that brain T_2 at 4.7 T is shorter than that at 1.5 and 3 T. Recently, Baron et al. found reduced diffusion contrast in stroke patients under short diffusion times (63). Latt et al. showed that DWI acquired with long diffusion time is susceptible to intra- and extra-cellular water exchange, especially in regions with compromised cell membranes (64). In addition, tissue with intact but functionally impaired and nearly impermeable membranes shows significantly reduced ADC. Consequently, long diffusion time may enhance diffusion contrast with elevated heterogeneity, for which the proposed ICON analysis might provide crucial information for tissue characterization. To summarize, the proposed relaxation-normalized fast kurtosis imaging is promising to aid the evaluation of fast DKI and its translation to the acute stroke setting.

5. CONCLUSION

Our study demonstrated that fast kurtosis imaging with Inherent COrrelation-based Normalization (ICON) reasonably corrects for the intrinsic regional kurtosis variation, enabling automatic segmentation of ischemic kurtosis lesion. We confirmed significant kurtosis/diffusivity lesion mismatch, which is a promising approach to elucidate the diagnostic value of fast DKI in acute stroke prior to its translation to the clinical setting.

Acknowledgments

The study was supported in part by grants from National Natural Science Foundation of China 81471721 (Guo), National Basic Research Program of China 2011CB70780420 (Ji), National Institute of Neurological Disorders and Stroke, National Institute of Health, 1R21NS085574 (Sun) and 1R01NS083654 (Sun). The authors would like to thank Ms. Nicole Eusemann for editorial assistance.

ABBREVIATIONS

ADC	Apparent Diffusion Coefficient
CBF	Cerebral Blood Flow
COV	Coefficient of Variation
CSF	Cerebrospinal Fluid
DKI	Diffusion Kurtosis Imaging
DWI	Diffusion-weighted Imaging
EPI	Echo Planar Imaging
FA	Fractional Anisotropy
MCAO	Middle Cerebral Artery Occlusion
MD	Mean Diffusivity
MK	Mean Kurtosis
TE	Echo Time
TR	Repetition Time

References

1. Moseley M, Kucharczyk J, Mintorovitch J, Cohen Y, Kurhanewicz J, Derugin N, Asgari H, Norman D. Diffusion-weighted MR imaging of acute stroke: correlation with T2-weighted and magnetic susceptibility-enhanced MR imaging in cats. Am J Neuroradiol. 1990; 11(3):423–429. [PubMed: 2161612]
2. Mintorovitch J, Moseley ME, Chileuitt L, Shimizu H, Cohen Y, Weinstein PR. Comparison of diffusion- and T2-weighted MRI for the early detection of cerebral ischemia and reperfusion in rats. Magn Reson Med. 1991; 18(1):39–50. [PubMed: 2062240]
3. Chien D, Kwong KK, Gress DR, Buonanno FS, Buxton RB, Rosen BR. MR diffusion imaging of cerebral infarction in humans. Am J Neuroradiol. 1992; 13(4):1097–1102. discussion 1103–1095. [PubMed: 1636519]

4. Warach S, Chien D, Li W, Ronthal M, Edelman R. Fast magnetic resonance diffusion-weighted imaging of acute human stroke. Neurology. 1992; 42(9):1717–1723. [PubMed: 1513459]
5. Parsons MW, Barber PA, Chalk J, Darby DG, Rose S, Desmond PM, Gerraty RP, Tress BM, Wright PM, Donnan GA, Davis SM. Diffusion- and perfusion-weighted MRI response to thrombolysis in stroke. Ann Neurol. 2002; 51(1):28–37. [PubMed: 11782981]
6. Kidwell CS, Alger JR, Saver JL. Beyond mismatch: evolving paradigms in imaging the ischemic penumbra with multimodal magnetic resonance imaging. Stroke. 2003; 34(11):2729–2735. [PubMed: 14576370]
7. Davalos A, Blanco M, Pedraza S, Leira R, Castellanos M, Pumar JM, Silva Y, Serena J, Castillo J. The clinical-DWI mismatch: a new diagnostic approach to the brain tissue at risk of infarction. Neurology. 2004; 62(12):2187–2192. [PubMed: 15210880]
8. Lansberg MG, Thijs VN, Bammer R, Olivot J-M, Marks MP, Wechsler LR, Kemp S, Albers GW. The MRA-DWI Mismatch Identifies Patients With Stroke Who Are Likely to Benefit From Reperfusion. Stroke. 2008; 39(9):2491–2496. [PubMed: 18635861]
9. Vilas D, de la Ossa NP, Millán M, Capellades J, Dávalos A. Brainstem lesions in diffusion sequences of MRI can be reversible after arterial recanalization. Neurology. 2009; 73(10):813–815. [PubMed: 19738178]
10. Yoo AJ, Hakimelahi R, Rost NS, Schaefer PW, Hirsch JA, Gonzalez RG, Rabinov JD. Diffusion weighted imaging reversibility in the brainstem following successful recanalization of acute basilar artery occlusion. J NeuroIntervent Surg. 2010; 2(3):195–197.
11. Yamada R, Yoneda Y, Kageyama Y, Ichikawa K. Reversal of large ischemic injury on hyper-acute diffusion MRI. Case Rep Neurol. 2012; 4(3):177–180. [PubMed: 23185171]
12. Sobesky J. Refining the mismatch concept in acute stroke: lessons learned from PET and MRI. J Cereb Blood Flow Metab. 2012; 32(7):1416–1425. [PubMed: 22510604]
13. Hossmann KA. Viability thresholds and the penumbra of focal ischemia. Ann Neurol. 1994; 36(4): 557–565. [PubMed: 7944288]
14. Geisler BS, Brandhoff F, Fiehler J, Saager C, Speck O, Rother J, Zeumer H, Kucinski T. Blood-oxygen-level-dependent MRI allows metabolic description of tissue at risk in acute stroke patients. Stroke. 2006; 37(7):1778–1784. [PubMed: 16741186]
15. An H, Liu Q, Chen Y, Lin W. Evaluation of MR-Derived Cerebral Oxygen Metabolic Index in Experimental Hyperoxic Hypercapnia, Hypoxia, and Ischemia. Stroke. 2009; 40(6):2165–2172. [PubMed: 19359642]
16. Fiehler J, Foth M, Kucinski T, Knab R, von Bezold M, Weiller C, Zeumer H, Rother J. Severe ADC decreases do not predict irreversible tissue damage in humans. Stroke. 2002; 33(1):79–86. [PubMed: 11779893]
17. Ringer TM, Neumann-Haefelin T, Sobel RA, Moseley ME, Yenari MA. Reversal of early diffusion-weighted magnetic resonance imaging abnormalities does not necessarily reflect tissue salvage in experimental cerebral ischemia. Stroke. 2001; 32(10):2362–2369. [PubMed: 11588327]
18. Nicoli F, Lefur Y, Denis B, Ranjeva JP, Confort-Gouny S, Cozzone PJ. Metabolic counterpart of decreased apparent diffusion coefficient during hyperacute ischemic stroke: a brain proton magnetic resonance spectroscopic imaging study. Stroke. 2003; 34(7):e82–87. [PubMed: 12817104]
19. Labeyrie M-A, Turc G, Hess A, Hervo P, Mas J-L, Meder J-Fo, Baron J-C, Touze E, Oppenheim C. Diffusion Lesion Reversal After Thrombolysis: A MR Correlate of Early Neurological Improvement. Stroke. 2012; 43(11):2986–2991. [PubMed: 22996954]
20. Kidwell CS, Jahan R, Gornbein J, Alger JR, Nenov V, Ajani Z, Feng L, Meyer BC, Olson S, Schwamm LH, Yoo AJ, Marshall RS, Meyers PM, Yavagal DR, Wintermark M, Guzy J, Starkman S, Saver JL. A Trial of Imaging Selection and Endovascular Treatment for Ischemic Stroke. N Engl J Med. 2013; 368(10):914–923. [PubMed: 23394476]
21. Jensen JH, Falangola MF, Hu C, Tabesh A, Rapalino O, Lo C, Helpern JA. Preliminary observations of increased diffusional kurtosis in human brain following recent cerebral infarction. NMR Biomed. 2011; 24(5):452–457. [PubMed: 20960579]

22. Falangola MF, Jensen JH, Babb JS, Hu C, Castellanos FX, Di Martino A, Ferris SH, Helpern JA. Age-related non-Gaussian diffusion patterns in the prefrontal brain. J Magn Reson Imaging. 2008; 28(6):1345–1350. [PubMed: 19025941]

23. Cheung MM, Hui ES, Chan KC, Helpern JA, Qi L, Wu EX. Does diffusion kurtosis imaging lead to better neural tissue characterization? A rodent brain maturation study. Neuroimage. 2009; 45(2): 386–392. [PubMed: 19150655]

24. Raab P, Hattingen E, Franz K, Zanella FE, Lanfermann H. Cerebral gliomas: diffusional kurtosis imaging analysis of microstructural differences. Radiology. 2010; 254(3):876–881. [PubMed: 20089718]

25. Wu EX, Cheung MM. MR diffusion kurtosis imaging for neural tissue characterization. NMR Biomed. 2010; 23(7):836–848. [PubMed: 20623793]

26. Wang JJ, Lin WY, Lu CS, Weng YH, Ng SH, Wang CH, Liu HL, Hsieh RH, Wan YL, Wai YY. Parkinson Disease: Diagnostic Utility of Diffusion Kurtosis Imaging. Radiology. 2011; 261(1): 210–217. [PubMed: 21771952]

27. Helpern JA, Adisetiyo V, Falangola MF, Hu C, Di Martino A, Williams K, Castellanos FX, Jensen JH. Preliminary evidence of altered gray and white matter microstructural development in the frontal lobe of adolescents with attention-deficit hyperactivity disorder: a diffusional kurtosis imaging study. J Magn Reson Imaging. 2011; 33(1):17–23. [PubMed: 21182116]

28. Grinberg F, Farrher E, Kaffanke J, Oros-Peusquens A-M, Shah NJ. Non-Gaussian diffusion in human brain tissue at high b-factors as examined by a combined diffusion kurtosis and biexponential diffusion tensor analysis. NeuroImage. 2011; 57(3):1087–1102. [PubMed: 21596141]

29. Blockx I, De Groof G, Verhoye M, Van Audekerke J, Raber K, Poot D, Sijbers J, Osmand AP, Von HÃrsten S, Van der Linden A. Microstructural changes observed with DKI in a transgenic Huntington rat model: Evidence for abnormal neurodevelopment. NeuroImage. 2012; 59(2):957–967. [PubMed: 21906685]

30. Grossman EJ, Ge Y, Jensen JH, Babb JS, Miles L, Reaume J, Silver JM, Grossman RI, Inglese M. Thalamus and Cognitive Impairment in Mild Traumatic Brain Injury: A Diffusional Kurtosis Imaging Study. J Neurotrauma. 2012; 29(13):2318–2327. [PubMed: 21639753]

31. Hui ES, Fieremans E, Jensen JH, Tabesh A, Feng W, Bonilha L, Spampinato MV, Adams R, Helpern JA. Stroke Assessment With Diffusional Kurtosis Imaging. Stroke. 2012; 43(11):2968–2973. [PubMed: 22933581]

32. Cheung JS, Wang E, Lo EH, Sun PZ. Stratification of heterogeneous diffusion MRI ischemic lesion with kurtosis imaging – Evaluation of mean diffusion and kurtosis MRI mismatch in an animal model of transient focal ischemia. Stroke. 2012; 43(8):2252–2254. [PubMed: 22773558]

33. Hansen B, Lund TE, Sangill R, Jespersen SN. Experimentally and computationally fast method for estimation of a mean kurtosis. Magn Reson Med. 2013; 69(6):1754–1760. [PubMed: 23589312]

34. Hansen B, Lund TE, Sangill R, Jespersen SN. Erratum: Hansen, Lund, Sangill, and Jespersen. Experimentally and Computationally Fast Method for Estimation of a Mean Kurtosis. Magnetic Resonance in Medicine 69:1754–1760 (2013). Magn Reson Med. 2014; 71(6):2250.

35. Tietze A, Hansen MB, Ostergaard L, Jespersen SN, Sangill R, Lund TE, Geneser M, Hjelm M, Hansen B. Mean Diffusional Kurtosis in Patients with Glioma: Initial Results with a Fast Imaging Method in a Clinical Setting. Am J Neuroradiol. 2015; 36(8):1472–1478. [PubMed: 25977481]

36. Sun PZ, Wang Y, Mandeville E, Chan S-T, Lo EH, Ji X. Validation of fast diffusion kurtosis MRI for imaging acute ischemia in a rodent model of stroke. NMR in Biomed. 2014; 27(11):1413–1418.

37. Wu Y, Kim J, Chan ST, Zhou IY, Guo Y, Igarashi T, Zheng H, Guo G, Sun PZ. Comparison of image sensitivity between conventional tensor-based and fast diffusion kurtosis imaging protocols in a rodent model of acute ischemic stroke. NMR Biomed. 2016; 29(5):625–630. [PubMed: 26918411]

38. Hansen B, Lund TE, Sangill R, Stubbe E, Finsterbusch J, Jespersen SN. Experimental considerations for fast kurtosis imaging. Magn Reson Med. 2015

39. Jensen JH, Helpern JA. MRI quantification of non-Gaussian water diffusion by kurtosis analysis. NMR Biomed. 2010; 23(7):698–710. [PubMed: 20632416]

40. Alsop DC, Detre JA. Multisection cerebral blood flow MR imaging with continuous arterial spin labeling. Radiology. 1998; 208(2):410–416. [PubMed: 9680569]
41. Williams DS, Detre JA, Leigh JS, Koretsky AP. Magnetic resonance imaging of perfusion using spin inversion of arterial water. Proceedings of the National Academy of Sciences of the United States of America. 1992; 89(1):212–216. [PubMed: 1729691]
42. Juang L-H, Wu M-N. MRI brain lesion image detection based on color-converted K-means clustering segmentation. Measurement. 2010; 43(7):941–949.
43. Jespersen SN, Lundell H, Sonderby CK, Dyrby TB. Orientationally invariant metrics of apparent compartment eccentricity from double pulsed field gradient diffusion experiments. NMR Biomed. 2013; 26(12):1647–1662. [PubMed: 24038641]
44. Glenn GR, Helpern JA, Tabesh A, Jensen JH. Quantitative assessment of diffusional kurtosis anisotropy. NMR Biomed. 2015; 28(4):448–459. [PubMed: 25728763]
45. Hansen B, Jespersen SN. Kurtosis fractional anisotropy, its contrast and estimation by proxy. Scientific reports. 2016; 6:23999. [PubMed: 27041679]
46. Lin W, Paczynski RP, Venkatesan R, He YY, Powers WJ, Hsu CY, Haacke EM. Quantitative regional brain water measurement with magnetic resonance imaging in a focal ischemia model. Magn Reson Med. 1997; 38(2):303–310. [PubMed: 9256112]
47. Schmierer K, Scaravilli F, Altmann DR, Barker GJ, Miller DH. Magnetization transfer ratio and myelin in postmortem multiple sclerosis brain. Ann Neurol. 2004; 56(3):407–415. [PubMed: 15349868]
48. Jensen JH, Helpern JA, Ramani A, Lu H, Kaczynski K. Diffusional kurtosis imaging: The quantification of non-gaussian water diffusion by means of magnetic resonance imaging. Magn Reson Med. 2005; 53(6):1432–1440. [PubMed: 15906300]
49. Dijkhuizen RM, de Graaf RA, Tulleken KA, Nicolay K. Changes in the diffusion of water and intracellular metabolites after excitotoxic injury and global ischemia in neonatal rat brain. J Cereb Blood Flow Metab. 1999; 19(3):341–349. [PubMed: 10078886]
50. Sehy JV, Ackerman JJ, Neil JJ. Apparent diffusion of water, ions, and small molecules in the Xenopus oocyte is consistent with Brownian displacement. Magn Reson Med. 2002; 48(1):42–51. [PubMed: 12111930]
51. van Pul C, Jennekens W, Nicolay K, Kopinga K, Wijn PF. Ischemia-induced ADC changes are larger than osmotically-induced ADC changes in a neonatal rat hippocampus model. Magn Reson Med. 2005; 53(2):348–355. [PubMed: 15678540]
52. Kettunen MI, Grohn OH, Lukkarinen JA, Vainio P, Silvennoinen MJ, Kauppinen RA. Interrelations of T(1) and diffusion of water in acute cerebral ischemia of the rat. Magn Reson Med. 2000; 44(6): 833–839. [PubMed: 11108619]
53. Jokivarsi KT, Hiltunen Y, Grohn H, Tuunanen P, Grohn OH, Kauppinen RA. Estimation of the onset time of cerebral ischemia using T1rho and T2 MRI in rats. Stroke. 2010; 41(10):2335–2340. [PubMed: 20814006]
54. Koenig SH, Brown RD 3rd, Spiller M, Lundbom N. Relaxometry of brain: why white matter appears bright in MRI. Magn Reson Med. 1990; 14(3):482–495. [PubMed: 2355830]
55. Lutti A, Dick F, Sereno MI, Weiskopf N. Using high-resolution quantitative mapping of R1 as an index of cortical myelination. Neuroimage. 2014; 93(Pt 2):176–188. [PubMed: 23756203]
56. Koenig SH. Cholesterol of myelin is the determinant of gray-white contrast in MRI of brain. Magn Reson Med. 1991; 20(2):285–291. [PubMed: 1775053]
57. Gelman N, Ewing JR, Gorell JM, Spickler EM, Solomon EG. Interregional variation of longitudinal relaxation rates in human brain at 3. 0 T: relation to estimated iron and water contents. Magn Reson Med. 2001; 45(1):71–79. [PubMed: 11146488]
58. Sun PZ, Wang E, Cheung JS. Imaging acute ischemic tissue acidosis with pH-sensitive endogenous amide proton transfer (APT) MRI – Correction of tissue relaxation and concomitant RF irradiation effects toward mapping quantitative cerebral tissue pH. Neuroimage. 2012; 60(1):1–6. [PubMed: 22178815]
59. Sun PZ, Cheung JS, Wang EF, Lo EH. Association between pH-weighted endogenous amide proton chemical exchange saturation transfer MRI and tissue lactic acidosis during acute ischemic stroke. J Cereb Blood Flow Metab. 2011; 31(8):1743–1750. [PubMed: 21386856]

60. Stanisz GJ, Odrobina EE, Pun J, Escaravage M, Graham SJ, Bronskill MJ, Henkelman RM. T1, T2 relaxation and magnetization transfer in tissue at 3T. Magn Reson Med. 2005; 54(3):507–512. [PubMed: 16086319]

61. Doerr A. Imaging: Fingerprinting with MRI. Nat Meth. 2013; 10(5):380–381.

62. Sicard K, Fisher M. Animal models of focal brain ischemia. Exp Transl Stroke Med. 2009; 1(1):7. [PubMed: 20150985]

63. Baron CA, Kate M, Gioia L, Butcher K, Emery D, Budde M, Beaulieu C. Reduction of Diffusion-Weighted Imaging Contrast of Acute Ischemic Stroke at Short Diffusion Times. Stroke. 2015; 46(8):2136–2141. [PubMed: 26152297]

64. Latt J, Nilsson M, van Westen D, Wirestam R, Stahlberg F, Brockstedt S. Diffusion-weighted MRI measurements on stroke patients reveal water-exchange mechanisms in sub-acute ischaemic lesions. NMR in biomedicine. 2009; 22(6):619–628. [PubMed: 19306340]

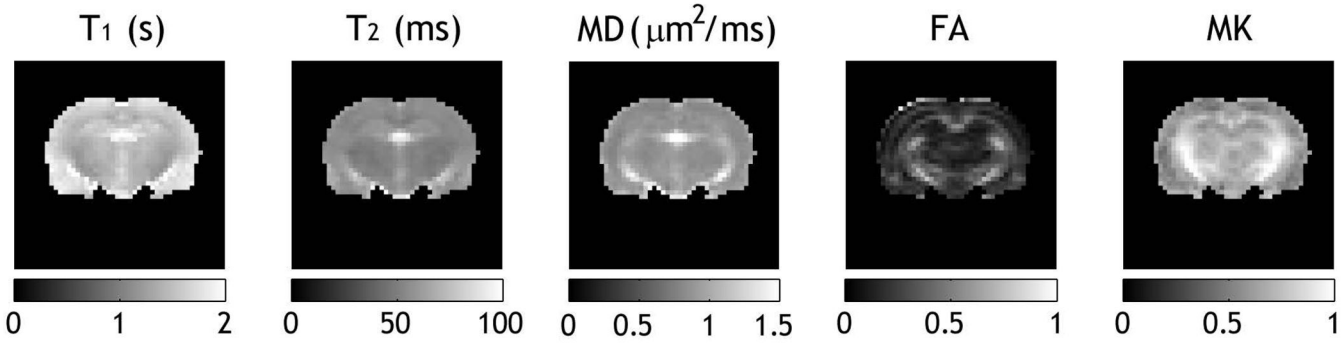

Fig 1.

Comparison of T_1, T_2, mean diffusivity (MD), fractional anisotropy (FA) and mean kurtosis (MK) maps of a representative normal rat.

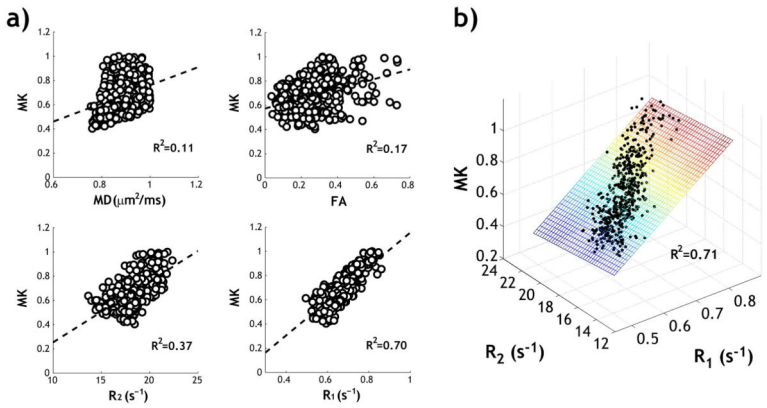

Fig 2.

a) Univariate linear regression analysis between mean kurtosis and multiple MRI indices, including MD, FA, R_2 (=1/T_2) and R_1 (=1/T_1) of a representative normal rat. **b)** Multiple linear regression analysis between mean kurtosis and R_1, R_2 of the same animal.

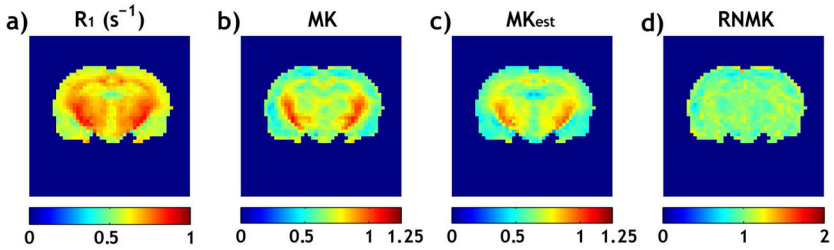

Fig 3.

Fast DKI with Inherent COrrelation-based Normalization (ICON) analysis in a representative normal rat. a) R_1 map. b) MK map with substantial regional variation. c) MK map estimated from R_1 map. d) Relaxation-normalized MK (RNMK) map ($RNMK=MK/MK_{est}$), which was substantially more homogeneous.

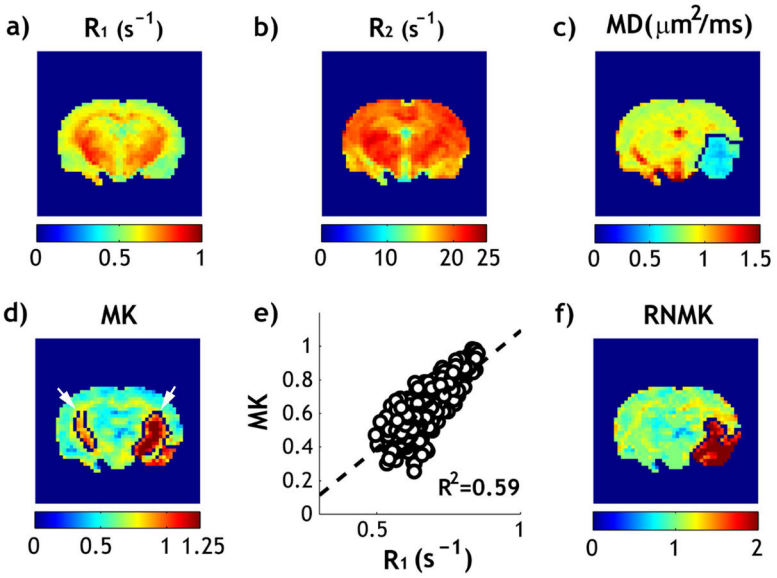

Fig 4.

Relaxation-normalized fast DKI of a representative rat after acute ischemic stroke. a) R_1 map. b) R_2 map. c) MD map with outlined ischemic lesion. d) MK map with outlined ischemic lesion. e) Linear regression analysis of R_1 and MK in the contralateral normal brain. f) RNMK map with outlined ischemic lesion.

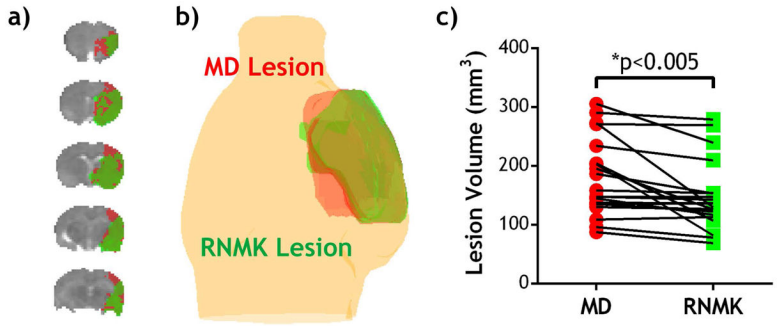

Fig 5.

Ischemic tissue segmentation using the proposed relaxation-normalized kurtosis MRI. a) MD lesion (red) vs. RNMK lesion (green). b) 3-D overlay of diffusion and kurtosis lesions. c) Comparison of ischemic diffusivity and kurtosis lesions.

Table 1

Comparisons of cerebral blood flow (CBF), MD and RNMK values in different brain regions.

N=20	Contralateral Normal Region	Diffusivity Lesion	Kurtosis Lesion	Kurtosis/Diffusivity Lesion Mismatch
CBF (ml/g/min)	1.27 ± 0.42	0.64 ± 0.40 ***	0.59 ± 0.37 ***	0.79 ± 0.51 **
MD (μm^2/ms)	0.86 ± 0.03	0.63 ± 0.06 ***	0.65 ±0.06 ***	0.68 ± 0.06 ***†
RNMK	1.00 ± 0.01	1.60 ± 0.27 ***	1.77 ± 0.21 ***§	1.17 ± 0.15 *§§§†††

One-way ANOVA with Bonferroni's multiple comparisons test was performed.

*** p<0.001,

** p<0.01,

* p<0.05 significantly different from contralateral normal region;

§§§ p<0.001,

§ p<0.05 significantly different from diffusivity lesion;

††† p<0.001,

† p<0.05 significantly different from kurtosis lesion. Note all the measurements passed D'Agostino-Pearson normality test, indicating Gaussian distribution.